

Article

Compressive Behaviors of High-Strength Geopolymeric Concretes: The Role of Recycled Fine Aggregate

Huaicheng Zhong¹, Huanchang Fu^{2,*}, Yuan Feng¹, Liming Li¹, Baifa Zhang¹, Zhanbiao Chen¹, Zhongyu Lu¹ and Jianhe Xie^{1,3,*}

¹ School of Civil and Transportation Engineering, Guangdong University of Technology, Guangzhou 510006, China; 2112209027@mail2.gdut.edu.cn (H.Z.); 1112109002@mail2.gdut.edu.cn (Y.F.); 2112009037@mail2.gdut.edu.cn (L.L.); zhangbaifa@gdut.edu.cn (B.Z.); zbchen@gdut.edu.cn (Z.C.); luzu@gdut.edu.cn (Z.L.)

² School of Civil Engineering and Architecture, Guangzhou Institute of Science and Technology, Guangzhou 510540, China

³ Guangdong AIB Polytechnic, Guangzhou 510507, China

* Correspondence: fhc@gzist.edu.cn (H.F.); jhxie@gdut.edu.cn (J.X.)

Abstract: In this study, natural fine aggregates (NFAs) in high-strength fly ash (FA)/ground granulated blast furnace slag (GGBFS)-based geopolymer concretes were both partially and completely replaced by RFAs to prepare geopolymer recycled fine aggregate concrete (GRFC). Herein, the impacts of RFA content (0%, 25%, 50%, 75%, and 100%) on the fresh and hardened performance and microstructural characteristics of a GRFC were investigated. The results indicated that with increasing RFA substitution ratio, the setting time of the GRFC decreases. In addition, the compressive strength and elastic modulus decrease. However, owing to the enhanced adhesion of the geopolymer matrix and recycled aggregate, RFA has a relatively small impact on the compressive strength, with a maximum strength loss of 9.7% at a replacement level of 75%. When the RFA content is less than 75%, the internal structure of the concrete remains relatively compact. The incorporation of RFA in concrete has been found to adversely affect its compressive strength and elastic modulus, while simultaneously increasing its brittleness. The increase in dosage of RFA leads to a reduction in the compressive strength and elastic modulus of concrete, while partial failure occurs when the GRFC constitutes 100% of the RFA. The existing stress–strain model for conventional concrete is recalibrated for the GRFC. Observed by SEM, with increasing RFA, the damage is mainly concentrated at the interface associated with the attached cement. Although the recalibrated model predicts the stress–strain responses of the GRFC reasonably well, an acceptable range of deviation is present when predicting the residual stress due to the relatively high strength and brittle behavior of the GRFC during compression. Through this research, the applicability of RFA is expanded, making it feasible to apply large quantities of this material.

Keywords: geopolymer concrete; recycled fine aggregate (RFA); stress–strain behavior; microstructure; prediction model



Citation: Zhong, H.; Fu, H.; Feng, Y.; Li, L.; Zhang, B.; Chen, Z.; Lu, Z.; Xie, J. Compressive Behaviors of High-Strength Geopolymeric Concretes: The Role of Recycled Fine Aggregate. *Buildings* **2024**, *14*, 1097. <https://doi.org/10.3390/buildings14041097>

Academic Editor: Flavio Stochino

Received: 26 March 2024

Revised: 9 April 2024

Accepted: 11 April 2024

Published: 15 April 2024



Copyright: © 2024 by the authors. Licensee MDPI, Basel, Switzerland. This article is an open access article distributed under the terms and conditions of the Creative Commons Attribution (CC BY) license (<https://creativecommons.org/licenses/by/4.0/>).

1. Introduction

Over the past two decades, global warming has attracted more attention than before. To reduce greenhouse gas emissions, many global leaders reached a consensus on energy conservation and emission reduction measures at the Paris Climate Change Conference [1]. In China, rapid economic growth has stimulated the development of the construction industry. The construction and use of buildings require the consumption of large amounts of resources and energy. In response to the demand for green and sustainable development, individuals in the construction industry should assume the responsibility of energy conservation and emission reduction [2,3]. Products of the cement industry account for 7% of the global emissions of anthropogenic CO₂ due to cement manufacturing [4]. During

cement manufacturing, carbon dioxide emissions are categorized into direct and indirect emissions. The calcination of calcium carbonate into limestone and the burning of fuel are classified as direct emissions, and the electrical energy consumed during production is classified as an indirect emission. This categorization suggests that cement manufacturing is a high-emission and energy-consuming industry that greatly impacts the environment [3]. To reduce carbon emission and energy consumption levels, scientists are constantly exploring new materials to replace cement. In 1908, a binder prepared by the reaction of alkali and solid aluminum silicate was patented. Today, this polymer, which is formed by the condensation of a silicon- and aluminum-rich raw material with a base, is called a geopolymer; this material exhibits high strength and good chemical resistance [5–7]. The raw materials for geopolymers come from industrial byproducts and solid waste. Thus, geopolymer concrete is considered a green and low-carbon concrete with development potential [8–10]. To date, many scholars have studied geopolymer concrete, the strength of which ranges from 20 to 80 MPa [11]. The work performance of geopolymer concrete and its influencing factors have been studied in terms of various aspects, thereby confirming its feasibility for replacing ordinary cement [12–14].

In addition, the construction of new buildings and the demolition of old buildings generate a large amount of construction waste, which is mainly handled by open piles and simple landfills to date, hence wasting resources while affecting the environment [15]. In this regard, the recycling of construction waste has been emphasized by many countries [16]. The rapid development of the construction industry in the past few decades has resulted in the exploitation of large quantities of river sand and natural gravel, thus increasing resource scarcity and greatly impacting the ecological environment. Recycled aggregates recovered from construction waste can solve the problems of waste disposal, resource conservation, and environmental protection [17]. Recently, research on the use of recycled aggregates in cementitious materials has been conducted. Xiao et al. [18], Silva et al. [19], and Guo et al. [20] summarized the research status of recycled aggregates and noted that recycled aggregates degrades the durability and mechanical properties of concrete. Achieving high strength with 100% recycled aggregates requires additional cement, which is detrimental to both the economy and carbon reduction measures [21]. The properties of recycled aggregates are influenced by the quality and amount of adherent mortar, and the low density and high water absorption attributes of adherent mortar can have a relatively great negative impact on concrete [22]. The use of recycled aggregates creates several different interfacial transition zones (ITZs), and some ITZs degrade the internal structure of concrete [23]. ITZs are thought to have a fundamental effect on the strength of concrete and are influenced by the quality of the adherent mortar [24,25]. However, geopolymers exhibit good bonding with natural aggregates and even better bonding with recycled aggregates. The unhydrated cement in the cement mortar adhered to recycled aggregates undergoes a secondary reaction in an alkaline environment, and a large amount of portlandite $[\text{Ca}(\text{OH})_2]$ is reduced to a dense C-S-H gel [26,27]. Therefore, recycled aggregates provide better results in geopolymer concrete.

In cement-based concrete, as the amount of recycled aggregate increases, the concrete exhibits poor mechanical properties [18,21,28,29]. In particular, the size of the recycled aggregate significantly affects the concrete strength. The smaller the size of the recycled aggregate is, the poorer the performance of the recycled concrete [30]. An important reason for this phenomenon is that the water absorption and adherent cement content of recycled aggregate both increase with decreasing recycled aggregate size [31,32]. Similarly, geopolymer recycled concrete shows a similar pattern of decreasing concrete strength with increasing recycled aggregate amount [26,33,34]. Compared to studies on geopolymer recycled coarse aggregate concrete, relatively few studies have been conducted on geopolymer recycled fine aggregate concrete (GRFC). In the study by Zhu et al. [35], when the substitution ratio of recycled fine aggregate (RFA) was less than 50%, the mechanical properties of mortar with RFA were similar to those of natural fine aggregate (NFA) mortar. This finding confirms the feasibility of replacing NFA with RFA

Therefore, in this study, GRFC was prepared using RFA to partially or completely replace NFA, focusing on the effects of RFA content (0%, 25%, 50%, and 100%) on the fresh and hardened properties of the GRFC. The effects of RFA on the stress–strain relationship of the GRFC were investigated. Scanning electron microscopy (SEM) was used to analyze the effect of RFA on the microstructure of the GRFC. In addition, a stress–strain prediction model and an elastic modulus prediction model for the GRFC were developed based on the prediction models from existing studies. In this study, the impact of RFA on geopolymer concrete is explored in detail and its extensive application is promoted.

2. Materials and Methods

2.1. Raw Materials

2.1.1. Precursors

In this study, ground granulated blast furnace slag (GGBFS) and fly ash (FA) were produced by Zhengzhou Yuanheng Environmental Protection Engineering. Figure 1 shows their micrographs and Table 1 shows their specific chemical compositions. According to the American Society for Testing and Materials (ASTM) C618 [36], the sum of the contents of SiO_2 , Al_2O_3 , and Fe_2O_3 in fly ash was 87.87%, and its CaO content was only 4.87%. Thus, this material belonged to class F.

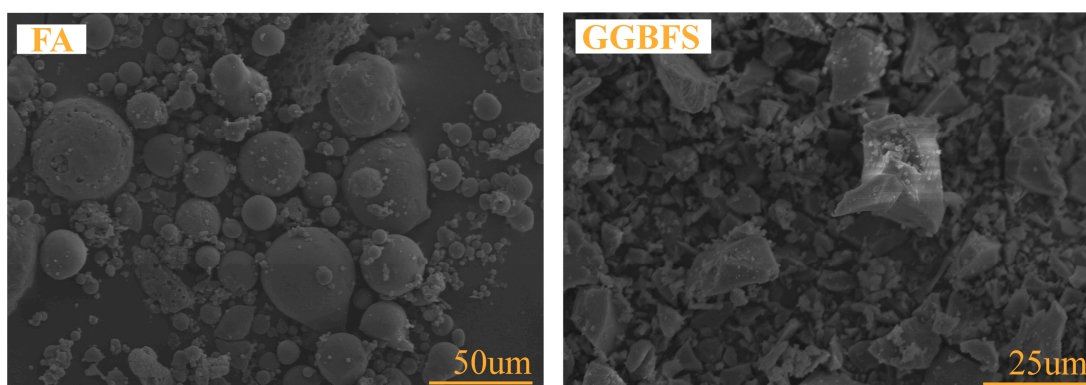


Figure 1. SEM images of precursors.

Table 1. Chemical compositions of GGBFS and FA (wt.%).

Precursor	SiO_2	Al_2O_3	CaO	Fe_2O_3	TiO_2	MgO	Others
FA	56.74	24.58	4.87	6.55	1.86	---	5.4
GGBFS	33.21	15.76	37.14	0.71	1.91	8.51	2.76

2.1.2. Alkaline Activators

Sodium hydroxide (NaOH) and sodium silicate (Na_2SiO_3) were used as alkaline activators in this test, and the activation mode was two-component activation. Table 2 shows the technical specifications of the excitants, where wt.% represents the percentage of each component in the total mass. Sodium silicate is a transparent viscous liquid. A sodium hydroxide solution was prepared by mixing a sodium hydroxide solid with water.

Table 2. Chemical composition of activators.

	Density (g/cm^3)	Na_2O (wt.%)	SiO_2 (wt.%)	H_2O (wt.%)
NaOH	1.32	18.78	-	81.22
Na_2SiO_3	1.384	8.9	28.8	62.2

2.1.3. Aggregates

All the coarse aggregates used in this study were natural coarse aggregates (NCAs), and the stone used was granite. The fine aggregates used were categorized into NFA and RFA. The RFA used in this study originated mainly from old highway renovation projects, and it was considered an ordinary Portland cement. RFA was then processed through several procedures, such as crushing, cleaning, wind selection, and sieving. In this study, fine particles with particle sizes ranging from 0.075 to 4.75 mm were selected as fine aggregates. The physical properties and sieving curves of the samples are detailed in Table 3 and Figure 2, where the water absorption level was that resulting from immersion for 2 h after absolute drying. Figure 2 shows that the particle gradations of the RFAs and river sand were basically the same, which could reduce the influences of differences in the gradations.

Table 3. Properties of aggregates.

	NFA	RFA	NCA
Grain size (mm)	0.075~4.75	0.075~4.75	5~20
Apparent density (g/cm ³)	2627.8	2558.1	2653.7
Water absorption (%)	0.83	10.53	0.9
Fineness modulus	1.64	1.64	--
Compression properties (%)	--	--	9.8

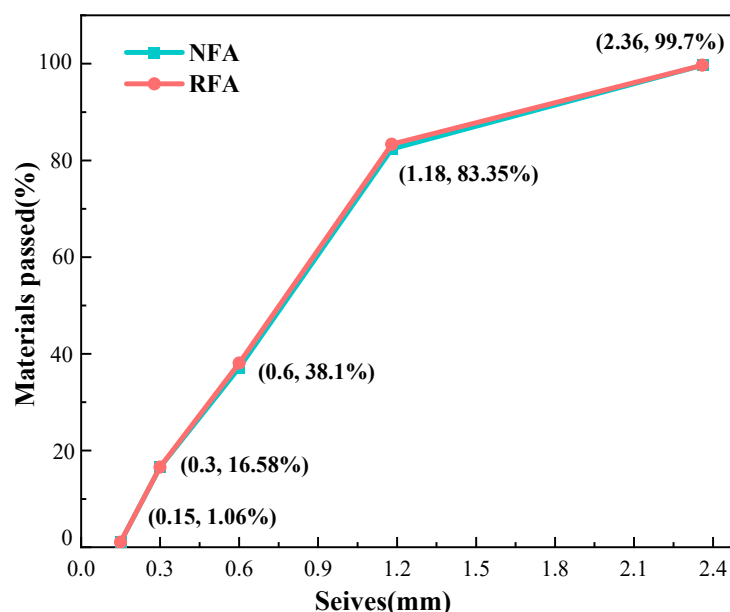


Figure 2. Particle size gradations of fine aggregates.

2.1.4. Admixture

According to related studies, GGBFS contains more CaO than other components, making it more active than other components and causing it to react rapidly when it encounters alkali solutions; thus, the setting time of geopolymers with a high proportion of GGBFS in the precursor is relatively short [27,37,38]. Without the addition of RFA, a retarder and a water reducer, the initial and final setting times of the sample were 7 min and 8 min, respectively, and these conditions could not satisfy the requirements of the working performance of concrete. In this study, by mixing a retarder and a water reducer into concrete, the initial and final setting times of slag-based aggregate concretes without RFAs were extended by 42 min and 47 min, respectively. First, polycarboxylic acid could

retard the reaction of fly ash/slag-based concrete [39,40]. Second, borax, as a retarder, reacted with calcium and silica to form a calcium-based borate inclusion layer in an alkali solution, which could separate the excited material from the exciter and slow the reaction process [41,42]. Scholars have suggested that the borate ions in the retardant could inhibit the dissolution of aluminum and silicon in the precursor because BO_4 could react with $[\text{SiO}_4]$ and replace $[\text{AlO}_4]$ in the (N,C)-A-S-H and C-S-H gels [43].

Therefore, sodium tetraborate decahydrate ($\text{Na}_2\text{B}_4\text{O}_7 \cdot 10\text{H}_2\text{O}$) and polycarboxylic acid, which are highly efficient water reducers, were selected as retarder and water reducers, respectively, in this experiment to obtain concrete with an enhanced setting time and slump.

2.2. Experimental Design

2.2.1. Mixture Design

In the present study, we investigated the substitution of fine aggregate river sand in concrete with equal masses of RFA at different substitution ratios. The substitution levels were 0%, 25%, 50%, 75%, and 100%. As shown in Table 4, five groups of GRFCs were designed based on the substitution levels, and each group consisted of three specimens. Based on the high water absorption capacity of RFA, the aggregates were water compensated to prevent the transfer of water from the mixture to the porous aggregates and to avoid changes in the effective water-to-cement ratio [21,44]. The amount of additional water was 9.7% of the mass of the RFA so that the remaining water absorption of the RFA was similar to that of the natural fine aggregate.

Table 4. GRFC mixture design of each group (kg/m^3).

Mix	NCA	NFA	RFA	FA	GGBFS	NaOH	Na_2SiO_3	W	AW	B	S
GRFC0		495	0						0		
GRFC25		371.2	123.8						12		
GRFC50	1155	247.5	247.5	125	375	125.7	126.4	26.6	24	20	10
GRFC75		123.8	371.2						36		
GRFC100		0	495						48		

Notes: W is free water, AW is additional water, B is a retarder, S is a water reducer, GRFC0 represents GRFC with a substitution ratio of 0%.

Fly ash is less reactive, and a large amount of fly ash slows solidification and strength development. Unreacted fly ash tends to form defects after the matrix hardens, while slag has relatively high activity during the reaction process to form a matrix with great strength and a dense microstructure. However, excessive slag content in concrete can result in excessive shrinkage, shortened setting time, and reduced fluidity [27,45–47]. Moreover, considering the working performance of concrete and the influence of the water-to-cement ratio, the final GGBFS/FA was determined to be 3/1, and the water-to-binder ratio was 0.4 [27,47]. According to the literature, two-component activation with an alkali dosage of 7% was used in this experiment, in which the two alkali solutions were mixed with $\text{SiO}_2/\text{Na}_2\text{O}$ at a ratio of 0.95 [27,48–50].

2.2.2. Preparation Methods

In this study, the mixing of aggregates and binder materials was performed in steps, and the process is shown in Figure 3. The main operation involved mixing RFA with additional water to ensure that the aggregate was prewetted and homogeneous, after which the NCA and NFA were added to the mixer. Then FA, GGBFS, and retarder were added, ensuring that the retarder is uniformly dispersed during the mixing process to achieve an even distribution of the solid components. For the addition of water-containing materials, a portion of the free water could be used to dissolve the water reducer while mixing thoroughly until there were no solid particles. Then, NaOH, Na_2SiO_3 , the water reducer, and the remaining free water were poured into the mixer and mixed thoroughly. After mixing, the concrete was tested and molded simultaneously, and the specimens were

cured until the end of the ageing period. The experimental groups were each prepared with three cylinders measuring 100×200 mm.

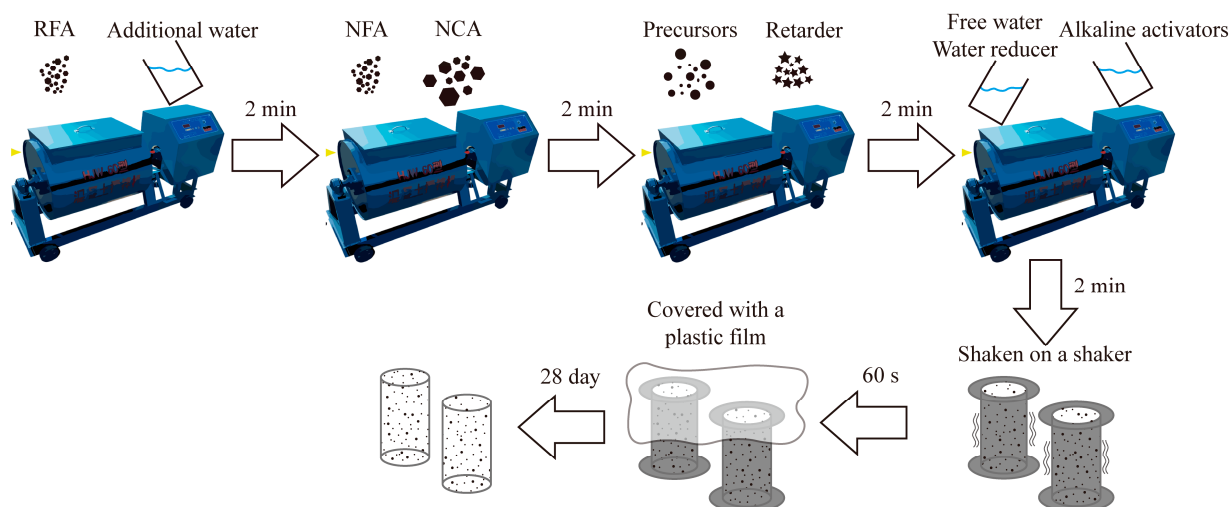


Figure 3. Preparation of GRFC.

2.3. Test Methods

2.3.1. Slump

The slumps of the GRFCs were determined according to the Chinese standard GB/T50080-2016 [51]. The base plate was placed on a flat bottom surface, the slump barrel was placed in the center of the base plate, and the base plate and barrel were moistened without stepping on the pedal of the cylinder to load the concrete into the barrel evenly three times. After each loading, the tamping rod was used to insert the tamping from the edge to the center in a spiral manner.

2.3.2. Setting Time

The setting times of the GRFCs were determined using a mortar setting time measuring instrument in accordance with the Chinese standard JGJ/T70-2009 [52]. To avoid the influence of coarse aggregate, the concrete was screened with a standard 4.75 mm sieve to remove the coarse aggregate, after which the mortar was left to determine the setting time.

2.3.3. Axial Compression Test

The loading equipment used for the test was a MATEST C088-01 material testing machine imported from Italy, with a maximum loading pressure of 4000 kN. This part of the test was in accordance with the ASTM C469-2017 [53]. The loading method involved displacement loading, and the loading rate was 0.18 mm/min.

Two axial and two circumferential resistive strain gauges (SGs) were set for each specimen. The axial strain gauges were parallel to the height direction of the specimen and symmetrically arranged. The circumferential strain gauges were perpendicular to the height of the specimen, located at the center of the specimen height, and symmetrically distributed. Moreover, a set of linear variable displacement transducers (LVDTs) was assembled parallel to the axial strain gages to measure the axial displacement of the strain gauges after failure, as shown in Figure 4.

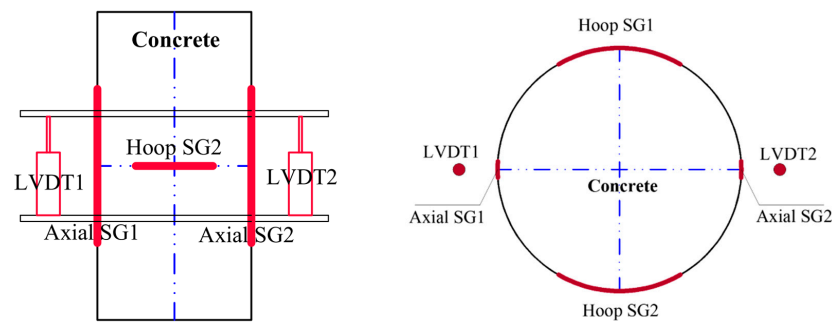


Figure 4. Test setup and instrumentation.

2.3.4. SEM

The raw materials and concrete matrix were sampled, dried for 24 h, and treated by spraying gold on the surface. The micromorphology of the sample was subsequently analyzed with an S-3400 N scanning electron microscope.

3. Results and Discussion

3.1. Fresh Properties

As shown in Figure 5, when the substitution ratio is less than 50%, the slump of the GRFC increases with increasing RFA content, and the concrete exhibits better workability. The reason for this change is that the prewetting of RFA leaves most of the aggregate in a saturated surface dry state, causing it to absorb little additional water for a short period during mixing and hydration. This phenomenon increases the slump of the concrete. Similar findings have been found in related experiments on geopolymer concrete [54,55]. However, when the substitution ratio is greater than 50%, the fluidity of the GRFC starts to decrease. The slump of concrete using 100% RFA is significantly lower than that of concrete without RFA. This inversion phenomenon is related to the hydrated cement attached to the RFA. Compared to recycled coarse aggregate, RFA adheres additional hydrated cement. As RFA substitution increases, additional adherent paste is incorporated into the concrete [32]. When prewetting RFA with additional water, the adherent paste absorbs water, causing the pores to leach a more alkaline pore fluid. This alkaline pore fluid is released during mixing of the concrete with additional water, thereby increasing the alkalinity of the concrete matrix. Some areas in strongly alkaline environments undergo a short hairline reaction period, resulting in a more viscous matrix with a reduced slump. Related studies have shown that slump decreases with increasing regeneration of aggregates [56].

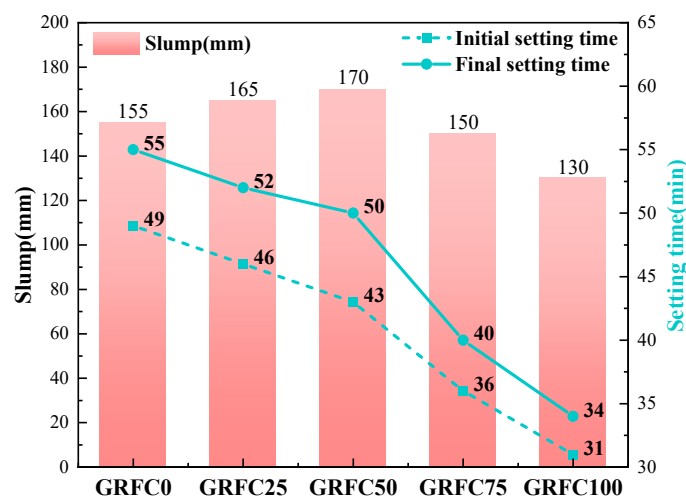


Figure 5. Effects of the substitution ratio of RFA on the slump and setting time of GRFCs.

As shown in Figure 5, the setting time of the GRFC decreases as the RFA substitution ratio increases. However, when the RFA substitution ratio exceeds 50%, the initial and final setting times of the GRFC with a 50% substitution ratio are reduced by 12.24% and 9.09%, whereas the initial and final setting times are reduced by 36.7% and 38.2%, respectively, when the substitution ratio is 100%. The main reason is the same as that for the slump change; the cement adhered to the RFA incorporated into the concrete increases the alkalinity of the matrix and advances the process of geopolymerizing GGBFS and FA so that the setting time is shortened [57,58]. In addition, the incorporation of adherent cement results in more calcium salts in the concrete, which accelerates the setting of concrete through heterogeneous nucleation [59].

3.2. Compressive Strength

The axial compressive strength is shown in Figure 6. Among the tested GRFCs, the concrete without RFA exhibits the highest compressive strength of 64.5 MPa. As the RFA substitution ratio increases, the strength decreases gradually. For the GRFC with 100% RFA, the strength decreases to 53.1 MPa. From the compressive strength loss ratio, with increasing RFA substitution ratio, the compressive strength loss ratio increases, and the maximum strength loss is 17.6%. When the RFA substitution ratio does not exceed 75%, the compressive strength decreases by only 9.7%. However, in the cement base, the GRFC with 100% RFA reduces the concrete compressive strength by as much as 30% [60,61]. Therefore, GRFC allows for the extensive utilization of RFA.

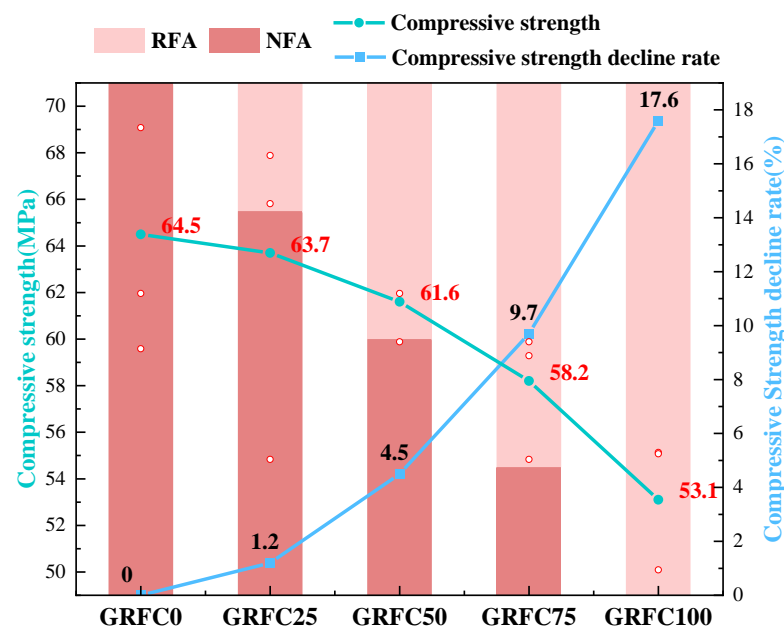


Figure 6. Effects of the substitution ratio of RFA on the compressive strengths of GRFCs.

The strength loss is attributed to the fact that the recycled aggregate used in this experiment is a cementitious concrete RFA with many defects and high porosity, deteriorating its mechanical properties [35]. Additionally, the addition of recycled aggregates makes multiple old and new transition zones within the concrete more numerous, weakening the bond between the matrix and the aggregate [57]. Compared to the results of previous studies, the decrease in strength of concrete can reach 20–30% after the addition of RFA [62]. However, the addition of RFA in this study has a reduced effect on the compressive strength of concrete. There are several reasons for this phenomenon. First, a reasonable dosage of the water-reducing agent polycarboxylic acid can effectively reduce water consumption, thus reducing the water-to-cement ratio and improving the strength of concrete [40]. Second, with the use of the retarder sodium tetraborate decahydrate, a reasonable dosage of borax positively affects the strength growth of fly ash/slag-based polymer concrete [42], because

the formation of the B-O bond in the structure mainly compensates for the difference and does not seriously impact the main C-(A)-S-H gel structure [63]. Third, for the unhydrated cement in cement mortar, the recycled aggregates adhere to secondary reactions in an alkaline environment, and $\text{Ca}(\text{OH})_2$ is reduced to a dense C-S-H gel, resulting in tight interactions between the recycled aggregates and the matrix [26,27]. However, due to the large amount of RFA, the bonding advantage of the transition zone is insufficient to compensate for the negative impact of RFA; thus, the compressive strength of the concrete still deteriorates.

3.3. Stress–Strain Relationship

The stress–strain curves of concrete at different substitution ratios of RFA are shown in Figure 7, where Figure 7f shows the representative curves of each substitution ratio placed together for comparative analysis.

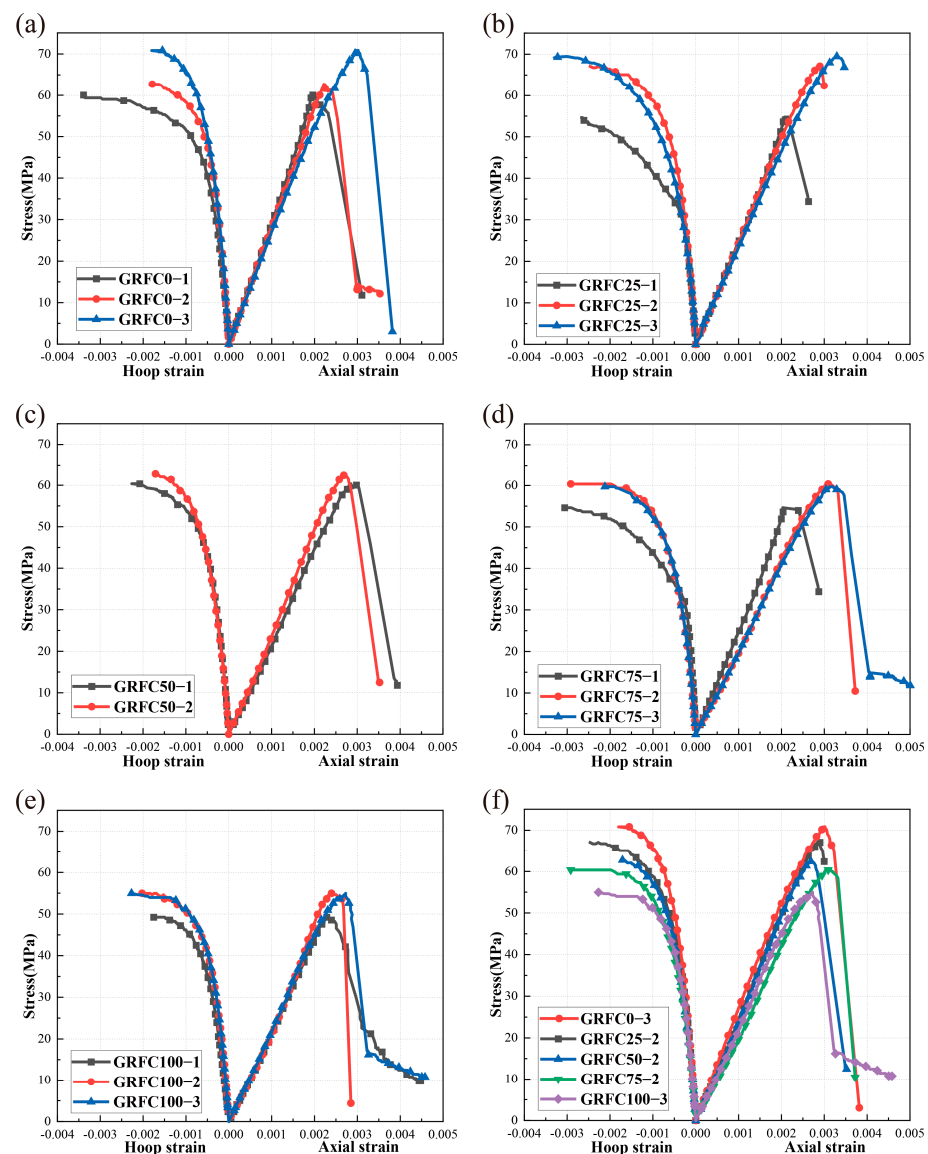


Figure 7. Stress–strain curves of GRFCs with different substitution ratio of RFA: (a) GRFC0, (b) GRFC25, (c) GRFC50, (d) GRFC75, (e) GRFC100, and (f) comparison of all GRFCs.

Figure 7 shows that the specimens in each group exhibit different degrees of brittle damage, with steep rising and falling segments, a fast loss of load-holding capacity after the stress peak, and rapid stress loss, which are similar to the experimental results of other

scholars [64,65]. This high stress peak and steep decline are associated with a relatively high content of GGBFS [27,38]. As shown in Figure 7f, the slopes of the peak and rising segments of the stress–strain curves of the concrete become progressively smaller as the RFA substitution ratio increases. When the substitution ratio exceeds 25%, the peak value and slope of the rising section of the curve start to change considerably. This change is influenced by the fact that the strength and elastic modulus of RFA are lower than those of natural fine aggregate [66]. With increasing substitution ratio, the slope of the descending section decreases gradually after the concrete reaches the peak stress. In addition, the stress loss accelerates, and the brittleness of the concrete increases. This phenomenon is caused by the cumulative amplification of many RFA defects [19,67]. Similarly, an increase in the substitution ratio of recycled coarse aggregate decreases the peak stress and increases the brittleness of geopolymer concrete [37].

3.4. Elastic Modulus

The elastic modulus of the cylindrical specimen can be calculated from the stress–strain curve by using Equation (1).

$$E = \frac{(S_2 - S_1)}{\epsilon_2 - 0.00005} \quad (1)$$

where

E is the elastic modulus of the GRFC.

S_2 is the stress corresponding to 40% of the ultimate load.

S_1 is the stress corresponding to a longitudinal axial stress.

ϵ_2 is the axial strain produced by stress S_2 .

As shown in Figure 8, the elastic modulus of the concrete exhibits a decreasing trend with increasing substitution ratio, decreasing by 14.5%, 19.8%, 23.7%, and 25.2%. The elastic modulus does not change much when the RFA substitution ratio is 50% or greater, and the main changes are concentrated before the substitution ratio reaches 25%. This finding shows that the RFA substitution ratio affects the elastic modulus of geopolymer recycled concrete to a more significant extent than the compressive strength. According to other cement-based studies, an increase in the substitution ratio of recycled aggregates significantly reduces the elastic modulus of concrete [62,68]. In related studies, researchers have shown that the elastic modulus of an aggregate is one of the most important factors affecting the elastic modulus of recycled concrete; this importance arises because recycled aggregates are more fragile and susceptible to damage than natural aggregates [19,69].

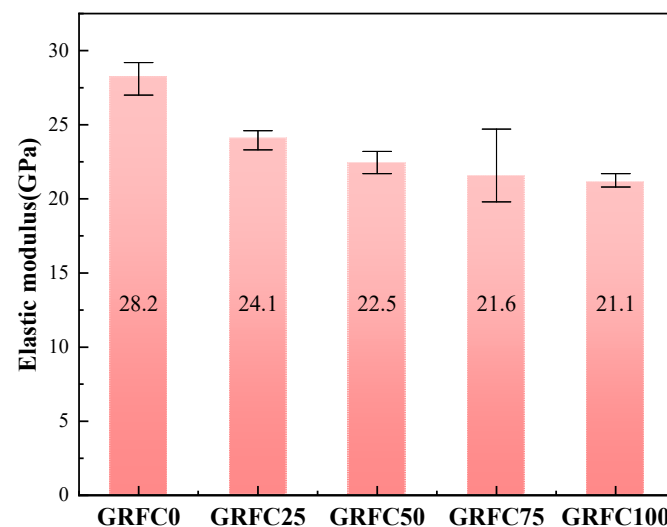


Figure 8. Effects of the substitution ratio of RFA on the elastic moduli of GRFCs.

3.5. Poisson's Ratio

The Poisson's ratio can be calculated with Equation (2). Figure 9 shows that the Poisson's ratio of the GRFC is 0.227 when the substitution ratio is 0. The Poisson's ratio of the GRFC continues to decrease within the range of 0.18–0.207 after incorporating RFA. The Poisson's ratio is minimized at an RFA substitution ratio of 75% to 0.18. The Poisson's ratio of the concrete slightly recovers when the substitution ratio reaches 100%, which is associated with the GRFC100 damage pattern.

$$\mu = \frac{(\varepsilon_{t2} - \varepsilon_{t1})}{\varepsilon_2 - 0.00005} \quad (2)$$

where

μ is the Poisson's ratio,

ε_{t2} is the transverse strain at the midheight of the specimen produced by stress S_2 .

ε_{t1} is the transverse strain at the midheight of the specimen produced by stress S_1 .

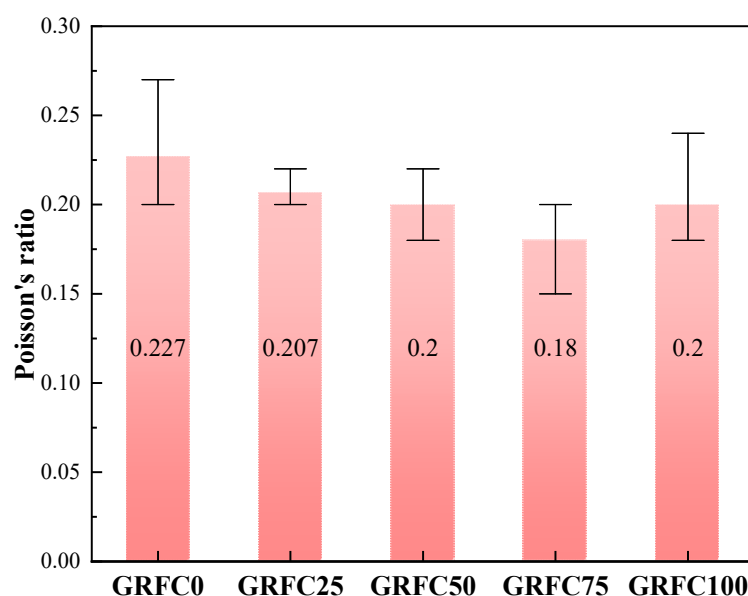


Figure 9. Effects of the substitution ratio of RFA on the Poisson's ratio of GRFCs.

3.6. Failure Mode

As shown in Figure 10, GRFC0 has no obvious penetrating large cracks. Furthermore, most small and long cracks span from the top to the bottom of the specimen, and falling concrete blocks do not appear. This phenomenon occurs because of the strong bond between cementitious materials and natural aggregates. In addition, the voids and defects are uniformly distributed in the concrete, which causes the cracks to be uniformly distributed [27]. GRFC25 exhibits penetrating large cracks, with a reduction in the number of small cracks. GRFC50 is damaged in a similar manner to GRFC25, but with the obvious appearance of falling concrete blocks and widening of the small cracks. GRFC75 cracks are mainly centered in the middle of the specimen, with additional small cracks dispersing along the main cracks. GRFC100 has a significantly smaller longitudinal damage area, which is concentrated where the cracks are generated. Moreover, the cracks are relatively short. Due to the high porosity, high number of defects, and low hardness of RFA [70], more defects appear in the concrete with increasing RFA admixture, changing the damage mode of cracks. In particular, when the RFA is substituted with 100%, the specimens appear to be characterized by local damage. The reason for this phenomenon is that there are excessive internal defects in the concrete. When a certain defect starts to cause damage, the cracks along the weak joints around the defects disperse rapidly [66,71]. Moreover, the bond

between the aggregates fails quickly. Under axial stress, the cracks do not have time to develop longitudinally, while the transverse interfaces are already stressed and damaged.



Figure 10. Failure modes of GRFCs.

During specimen compression, when the RFA substitution ratio is lower than 75%, the concrete reaches its ultimate peak, the concrete is damaged suddenly, and a large sound occurs. When the RFA substitution ratio is higher than 75%, the sound is weakened when the concrete is damaged. Combined with the experimental phenomena and damage results, these findings indicate that RFA substitution has a certain effect on concrete, especially in the case of full substitution, where the concrete damage mode obviously changes; however, when the RFA substitution ratio is lower than 75%, the concrete damage changes are small, making many applications of RFA feasible.

3.7. SEM Images

As shown in Figure 11, the aggregates, matrix, and cracks are labeled with existing relevant studies [27,54,72–75]. The figure shows that the surface of NFA is relatively smooth. Furthermore, the surface of RFA is rough and more angular and slightly whiter in appearance than that of virgin plants. As shown in the figure, for GRFC0, FA and GGBFS form a tight gel structure when excited by a high-alkali solution. According to the micrographs at different substitution ratios of RFA, as the RFA dosage increases, the concrete matrix becomes looser, more porous, and more prone to forming cracks than before.

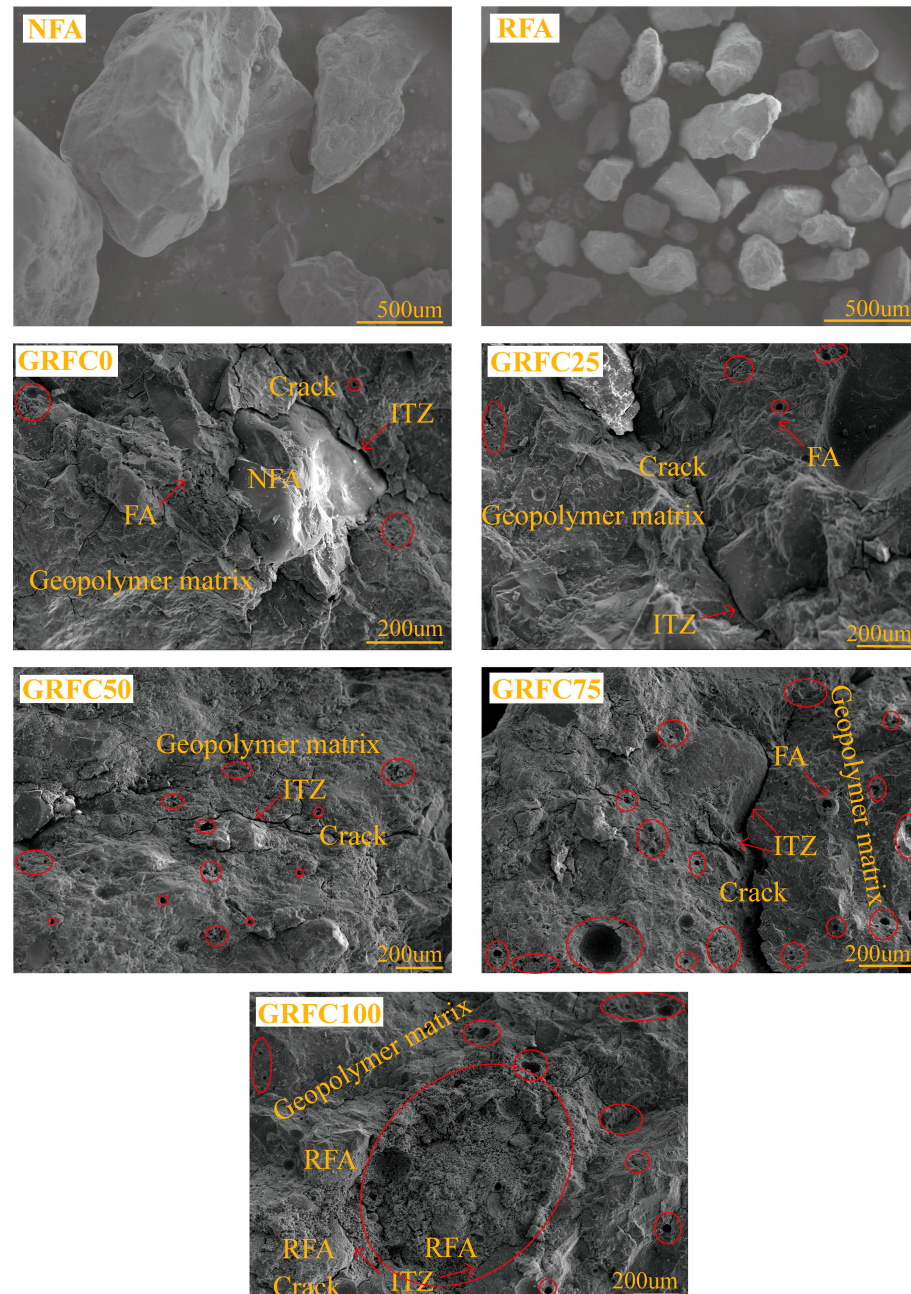


Figure 11. Microstructures of specimens with different substitution ratios of RFA.

A comparison of the SEM images of GRFC0 and GRFC25 reveals that the cracks all arise mainly from the transition surface between the aggregate and the matrix. With an increasing incorporation of RFA, the matrix exhibits a higher degree of porosity. Upon complete substitution of RFA, a distinct porous matrix becomes evident, indicating a loose

and weak bond between aggregates and geopolymer matrix. The full replacement of RFA introduces numerous such defects, resulting in a significant reduction in concrete strength and localized damage concentration.

A comprehensive analysis of the microscopic damage of geopolymer concrete under different substitution ratios of RFA was conducted. When the substitution ratio is less than 75%, the damage mainly arises from the ITZs between the aggregate and matrix. When the substitution ratio reaches and exceeds 75%, the damage begins to arise from the ITZ between the attached cement and geopolymer matrix.

4. Empirical Model

4.1. Elastic Modulus Model

As in Figure 12a, the results of the experiment are compared with the highly cited models of existing studies [76–79], which are cited in Table 5. These models are not applicable to this experiment. Moreover, from the change in elastic modulus of the experimental results, the change trend of the elastic modulus of the existing models is found to be inconsistent with the results of this experiment. Therefore, in this study, a new prediction model is fitted to the experimental results by drawing on the existing research models with the following Equation (3):

$$E_c = 0.0032(f_c)^{1.97} + 13.4 \quad (3)$$

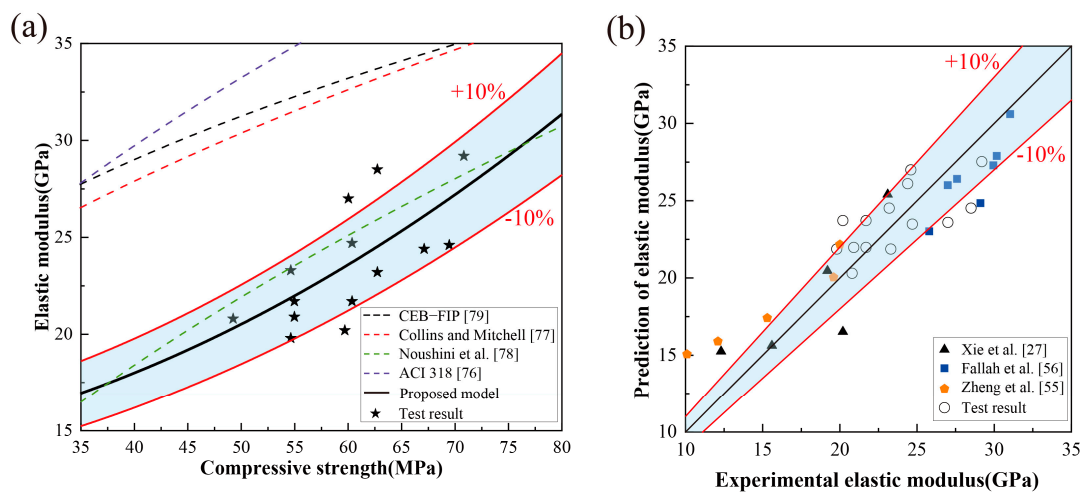


Figure 12. Existing elastic modulus models and data comparison. (a) Comparison of models. (b) Analysis of prediction effect. [27,55,56,76–79].

Table 5. Existing elastic modulus models.

References	Scope of Application	Formulas
CEB-FIP [79]	Normal-strength and high-strength concrete	$E_c = 0.85 \times 2.15 \times 10^4 (f_c/10)^{1/3}$ (4)
Collins and Mitchell [77]	Normal-strength and high-strength concrete	$E_c = 3320\sqrt{f_c} + 6900$ (5)
Noushini et al. [78]	Fly ash-based geopolymer concrete	$E_c = -11400 + 4712\sqrt{f_c}$ (6)
ACI 318 [76]	Normal-strength and high-strength concrete	$E_c = 4740(f_c)^{1/2}$ (7)

Notes: E_c : elastic modulus and f_c : compressive strength.

Figure 12a shows that most of the experimental results fall within the error range of $\pm 10\%$ of the fitted curve (blue shaded area); the trend of the curve is consistent with the trend of the experimental results, and the prediction model can effectively predict the elastic modulus of this experiment.

To further explore the elastic modulus prediction model of this study, the experimental results of other scholars are introduced for comparative analysis, as shown in Figure 12b.

The data introduced are all experimental data of recycled aggregate geopolymer concrete with fly ash and slag as precursors, all exhibiting high elastic moduli and strengths. Fallah et al. [56] and Xie et al. [27] used recycled coarse aggregate prepared from ordinary construction concrete waste, while Zheng et al. [55] used recycled brick aggregate. As shown in Figure 12b, most of the data points fall within the 10% error interval (blue shaded area). In particular, the experimental results from Fallah et al. [56] are effectively predicted by our prediction model. Like in the present study, in Fallah's study, more slag was used to achieve strengths of 50 MPa and above. However, unlike in the present study, in Fallah's study, recycled coarse aggregate was used for comparison. The experiments of Xie et al. [27] and Zheng et al. [55] used more fly ash and both used recycled coarse aggregate. According to the data from these two experiments, the present model has some predictive effect on the high-strength specimens but no significant predictive effect on the specimens with strengths below 45 MPa. Therefore, the elastic modulus model in this study has a better predictive effect for this experiment and some effect on predicting recycled aggregate ground polymer concrete with strengths higher than 45 MPa.

4.2. Stress–Strain Model

In this study, the stress–strain relationships of GRFCs with different RFA substitution ratios are constructed based on concrete stress–strain models widely used in existing studies and combined with the characteristics of this experiment. Table 6 shows the details of the selected existing models. Among them, the CEB–FIP [79], Collins and Mitchell [77], and Xiao et al. [80] models are all stress–strain models for ordinary Portland cement concrete, and are frequently referenced and cited in the present study. Noushini et al. [78] presented a stress–strain model for geopolymer concrete. Each model is shown in Figure 13, where the light blue area is the area enclosed by the stress–strain curves of the three specimens in each set of experiments, which is used to visualize the applicability of each model. The proposed model is that proposed in this study. In the model of Noushini et al. [78], due to the nature of the n_1 function, there is a range requirement for the ratio of E_{sec} to E_c , and the data of this experiment cannot meet the requirement of n_1 ; additionally, the model is borrowed from the Collins and Mitchell model. Therefore, the model is discarded.

Table 6. Existing stress–strain models.

Models	Stress–Strain Models	Parameter
CEB–FIP [79]	$y = (kx - x^2) / [1 + (k - 2)x],$ $0 \leq x \leq a$ $y = 1 / \left[\left(\frac{b}{a} - \frac{2}{a^2} \right) x^2 + \left(\frac{4}{a} - b \right) x \right],$ $a < x$	$k = E_C / E_{sec}$ $a = \frac{1}{2} \left(\frac{k}{2} + 1 \right) + \sqrt{\frac{1}{4} \left(\frac{k}{2} + 1 \right)^2 - \frac{1}{2}}$ $b = \frac{4[a^2(k-2)+2a-k]}{[a(k-2)+1]^2}$
Collins and Mitchell [77]	$y = \frac{nx}{n-1+x^{nm}}$	$n = 0.8 + \frac{f_{cm}}{17}$ $\text{when } y > 1, m = 0.67 + \frac{f_{cm}}{62}$ $\text{when } 0 \leq y \leq 1, m = 1$
Xiao et al. [80]	$y = c_1x + (3 - 2c_1)x^2 + (c_1 - 2)x^3,$ $0 \leq x \leq 1$ $y = x / \left[c_2(x - 1)^2 + x \right],$ $1 < x$	$c_1 = 2.2(0.748r^2 - 1.231r + 0.975)$ $c_2 = 0.8(7.6483r + 1.142)$
Noushini et al. [78]	$y = \frac{nx}{n-1+x^n}; 0 \leq x \leq 1, n = n_1;$ $1 \leq x, n = n_2$	$n_1 = \left(1.02 - 1.17 \frac{E_{sec}}{E_c} \right)^{-0.45}$ $n_2 = n_1 + d + 28e$ $d = 15(12.4 - 0.015f'_c)^{-0.5}$ $e = 0.83e^{-911/f_{cm}}$

Notes: $x = \frac{\epsilon_c}{\epsilon_0}$, $y = \frac{\sigma_c}{f_{cm}}$, E_c : elastic modulus, E_{sec} : secant modulus, σ_c : stress, ϵ_c : strain, f_{cm} : peak stress, and ϵ_0 : peak strain.

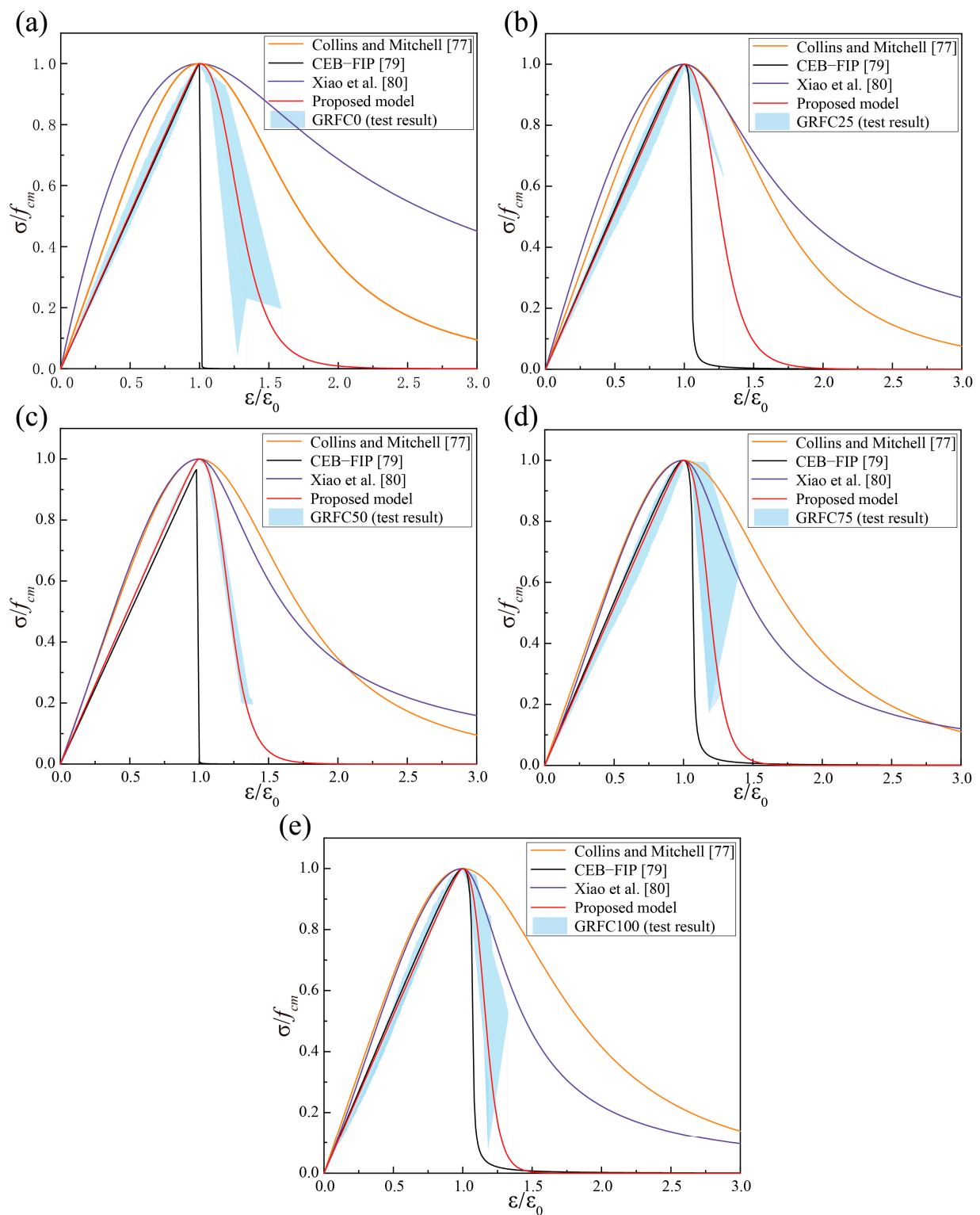


Figure 13. Comparison on existing and proposed stress–strain models with experimental results. (a) GRFC0. (b) GRFC25. (c) GRFC50. (d) GRFC75. (e) GRFC100. [77,79,80].

Figure 13 shows that the CEB–FIP model agrees well with the experimental results in the ascending section. However, this model underestimates the concrete in the descending section, which deviates greatly from the experimental results. The Collins and Mitchell and Xiao models deviate from the experimental results to different degrees in both the rising and falling segments. This finding indicates that the commonly used stress–strain

model for ordinary Portland cement is not applicable to highly brittle geopolymers. Therefore, by combining the characteristics of high strength and high brittleness shown in the stress–strain relationship in this experiment and the applicability of the cited models, we fit the relationship between the stress–strain curves of RFA and the GRFC based on the cited models. To obtain accurate results, the model is fitted in segments. In the ascending section, the functional equation of the CEB–FIP model, which is closer to the experimental results, is used to fit the experimental results. Furthermore, the coefficient of determination of the fitted results, R^2 , is greater than 0.987. Then, different parameter values, A , are obtained from different RFA substitution ratios; finally, the relationship between the RFA substitution ratio μ and A and the relationship between the stress and strain values of the GRFC are obtained from the regression analysis. For the descending section, the three models strongly deviate from the experimental results. After fitting the functional formulas of the three models and comparing and analyzing the applicability, the functional formulas of the Collins and Mitchell models are ultimately selected. The coefficients of determination of the fitted results, R^2 , are all greater than 0.911. Like in the ascending section, we can obtain the relationship between μ and the stress–strain of the GRFC. Therefore, the proposed model of this experiment is shown in Equation (12).

$$\begin{aligned} y &= \frac{Ax-x^2}{1+(A-2)x}, \quad 0 \leq x \leq 1, \quad A = 1.023 + 0.031\mu - 0.014\mu^2 \\ y &= \frac{Bx}{B-1+x^B}, \quad 1 \leq x, \quad B = 11.301 + 5.936\mu + 4.909\mu^2 \end{aligned} \quad (12)$$

where $x = \frac{\sigma_c}{f_{cm}}$, $y = \frac{\varepsilon_c}{\varepsilon_0}$, ε_0 : peak strain, f_{cm} : peak stress, σ_c : stress, ε_c : strain, and μ : RFA substitution ratio.

From Figure 13, the prediction model basically matches the experimental results, and the slope of the descending section decreases with increasing μ , which is in agreement with the results of the aforementioned stress–strain analysis. Therefore, the prediction model has a good predictive effect for this experiment. Conversely, the accuracy of the prediction still needs additional GRFC-related data for improvement.

As shown in Figure 14, to further explore the applicability of the stress–strain model proposed in this study, the experimental data of Chang et al. [81] and Li et al. [82] are cited in this study for comparison, both of which use recycled aggregates prepared from ordinary construction concrete waste. Chang et al. experimentally studied the effect of the recycled coarse aggregate substitution ratio on ordinary Portland cement, and the experimental groups with peak stresses that exceed 50 MPa are chosen to validate the stress–strain prediction model of this study. Li et al. experimentally studied the effect of the recycled coarse aggregate substitution ratio on slag geopolymer concrete. The quoted data are normalized and compared with the prediction model of this study. Clearly, in the rising section, the prediction model of this study has a good predictive effect on the slag geopolymer concrete of Li et al. In the falling section, the prediction model of this study predicts the changes in the two sets of cited experimental data very well, and it shows a high degree of fit. Therefore, the stress–strain prediction model of this study not only has a better prediction effect on the RFA high-slag geopolymer of this experiment, but also has a better prediction effect on the recycled coarse aggregate high-slag geopolymer concrete and high-strength (≥ 50 MPa) recycled coarse aggregate ordinary Portland cement, which is of great significance for the application of recycled aggregates in engineering.

Therefore, the stress–strain prediction model of this study has a better predictive effect on the RFA high-slag geopolymer, on the recycled coarse aggregate high-slag geopolymer concrete, and on the high-strength (≥ 50 MPa) recycled coarse aggregate ordinary Portland cement, which is highly important for the engineering of recycled aggregates.

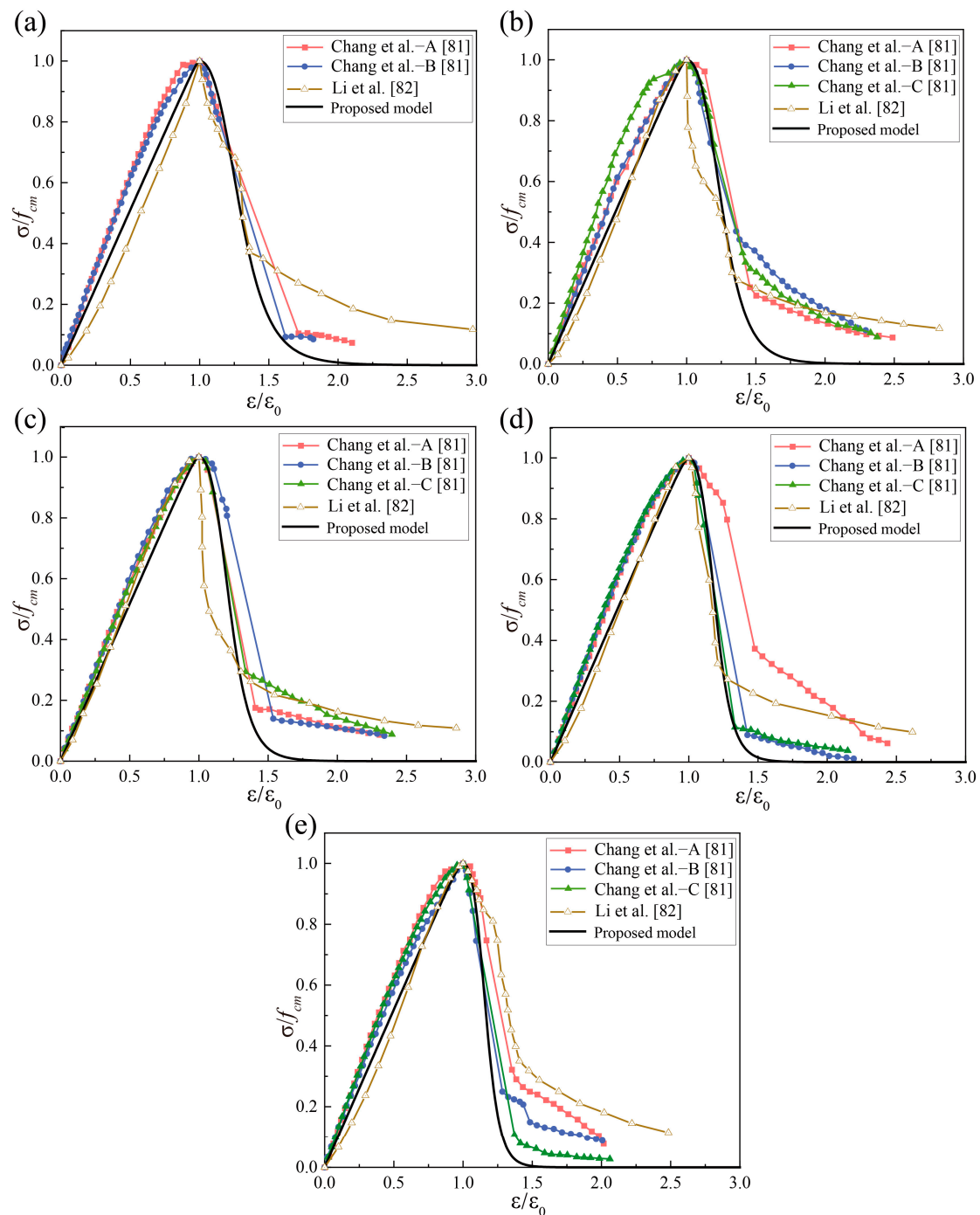


Figure 14. Comparison of the proposed model with experimental data from others' research. (a) Recycled aggregate 0%. (b) Recycled aggregate 25%. (c) Recycled aggregate 50%. (d) Recycled aggregate 75%. (e) Recycled aggregate 100%. [81,82].

5. Conclusions

In this paper, an experimental study on the effects of RFA on the properties of geopolymer concrete was reported. Compared with the existing recycled aggregate concrete research, the mechanism by which RFA could influence geopolymer concrete was analyzed. By combining the traditional concrete model with the experimental results, the elastic modulus prediction model and the stress–strain prediction model of the GRFC were obtained. The following conclusions could be drawn:

- (1) The incorporation of RFA has a significant impact on the fresh properties of the GRFC. The higher the quantity of added RFA is, the shorter the setting time of the GRFC. In addition, a moderate amount of RFA ($\leq 50\%$) can increase the fluidity of concrete. However, when the amount of RFA is more than 50%, the fluidity of concrete can become poor.
- (2) RFAs have good adhesion to the geopolymer matrix. When the RFA content is less than 75%, the internal structure of the concrete remains dense. The strength loss is within 9.7% at a substitution ratio of 75% of the RFA.
- (3) The high porosity and low strength of RFA reduce the compressive strength and elastic modulus of concrete and increase the brittleness of the concrete. Partial failure occurs when the GRFC is 100% of the RFA.
- (4) Damage to the concrete matrix is caused mainly by the ITZs between the aggregates and the matrix. With increasing RFA, the damage is mainly concentrated at the interface associated with the attached cement.
- (5) The proposed prediction model performs well in predicting the stress–strain response and ultimate point of high-strength (≥ 50 MPa) geopolymer concrete with recycled aggregate. However, there is bias in the prediction of the 30% residual stress after the peak. A more suitable functional formula can be used to describe the stress–strain relationship in future research on recycled aggregate concrete models.

In conjunction with the aforementioned research experiments, we put forth the subsequent recommendations:

- (1) The RFA content in the main structural parts can be adjusted between 50% and 75% based on specific requirements, resulting in enhanced operational performance while maintaining a strength reduction within 10%.
- (2) The RFA can be effectively utilized in non-structural components, exhibiting a strength of 53.1 MPa.

In this study, the impact of RFA on geopolymer concrete is explored in detail and its extensive application is promoted.

Author Contributions: Conceptualization, H.F.; Methodology, H.F., Y.F., L.L. and B.Z.; Software, H.Z. and Y.F.; Validation, L.L.; Formal analysis, H.Z. and Z.C.; Resources, J.X.; Data curation, H.Z., H.F. and L.L.; Writing—original draft, H.Z.; Writing—review & editing, H.F., Y.F., B.Z., Z.C., Z.L. and J.X.; Visualization, Z.L.; Supervision, B.Z., Z.L. and J.X.; Project administration, J.X.; Funding acquisition, J.X. All authors have read and agreed to the published version of the manuscript.

Funding: The authors gratefully acknowledge the financial support provided by the Science and Technology Planning Project of Guangdong Province (Grant No. 2022A0505050077), and the National Natural Science Foundation of China (Grant Nos. 12372180, 12072078).

Data Availability Statement: The original contributions presented in the study are included in the article, further inquiries can be directed to the corresponding authors.

Conflicts of Interest: The authors declare no conflict of interest.

References

1. Schellnhuber, H.-J. Why the right climate target was agreed in Paris. *Nat. Clim. Chang.* **2016**, *6*, 649–653. [[CrossRef](#)]
2. Liu, S.-W.; Tian, X.; Cai, W.-J.; Chen, W.-Q.; Wang, Y.-F. How the transitions in iron and steel and construction material industries impact China's CO₂ emissions: Comprehensive analysis from an inter sector linked perspective. *Appl. Energy* **2018**, *211*, 64–75. [[CrossRef](#)]
3. Ali, M.-B.; Saidur, R.; Hossain, M.-S. A review on emission analysis in cement industries. *Renew. Sustain. Energy Rev.* **2011**, *15*, 2252–2261. [[CrossRef](#)]
4. Deja, J.; Uliasz-Bochenczyk, A.; Mokrzycki, E. CO₂ emissions from Polish cement industry. *Int. J. Greenh. Gas Control.* **2010**, *4*, 583–588. [[CrossRef](#)]
5. Duxson, P.; Fernández-Jiménez, A.; Provis, J.-L.; Lukey, G.-C.; Palomo, A.; van Deventer, J.-S.J. Geopolymer technology: The current state of the art. *J. Mater. Sci.* **2007**, *42*, 2917–2933. [[CrossRef](#)]
6. Singh, B.; Ishwarya, G.; Gupta, M.; Bhattacharyya, S.-K. Geopolymer concrete: A review of some recent developments. *Constr. Build. Mater.* **2015**, *85*, 78–90. [[CrossRef](#)]

7. Chen, F.-M.; Zhao, J.-X.; Zhong, H.-C.; Feng, Y.; Chen, C.-G.; Xie, J.-H. An investigation of the durability of ultra-lightweight high-strength geopolymeric composites. *J. Build. Eng.* **2023**, *80*, 107990. [[CrossRef](#)]
8. Mehta, A.; Siddique, R. An overview of geopolymers derived from industrial by-products. *Constr. Build. Mater.* **2016**, *127*, 183–198. [[CrossRef](#)]
9. Li, Z.-M.; Delsaute, B.; Lu, T.-S.; Kostiuchenko, A.; Staquet, S.; Ye, G. A comparative study on the mechanical properties, autogenous shrinkage and cracking proneness of alkali-activated concrete and ordinary Portland cement concrete. *Constr. Build. Mater.* **2021**, *292*, 123418. [[CrossRef](#)]
10. Zhang, Z.-H.; Yao, X.; Zhu, H.-J. Potential application of geopolymers as protection coatings for marine concrete II. Microstructure and anticorrosion mechanism. *Appl. Clay Sci.* **2010**, *49*, 7–12. [[CrossRef](#)]
11. Luo, Z.-Y.; Li, W.-G.; Wang, K.-J.; Castel, A.; Shah, S.-P. Comparison on the properties of ITZs in fly ash-based geopolymer and Portland cement concretes with equivalent flowability. *Cem. Concr. Res.* **2021**, *143*, 106392. [[CrossRef](#)]
12. Peng, Y.-Q.; Zheng, D.-P.; Pan, H.-S.; Yang, J.-L.; Lin, J.-H.; Lai, H.-M.; Wu, P.-Z.; Zhu, H.-Y. Strain hardening geopolymer composites with hybrid POM and UHMWPE fibers: Analysis of static mechanical properties, economic benefits, and environmental impact. *J. Build. Eng.* **2023**, *76*, 107315. [[CrossRef](#)]
13. Chen, G.; Zheng, D.-P.; Chen, Y.-W.; Lin, J.-X.; Lao, W.-J.; Guo, Y.-C.; Chen, Z.-B.; Lan, X.-W. Development of high performance geopolymer concrete with waste rubber and recycle steel fiber: A study on compressive behavior, carbon emissions and economical performance. *Constr. Build. Mater.* **2023**, *393*, 131988. [[CrossRef](#)]
14. Li, L.-M.; Xie, J.-H.; Zhang, B.-F.; Feng, Y.; Yang, J. A state-of-the-art review on the setting behaviours of ground granulated blast furnace slag- and metakaolin-based alkali-activated materials. *Constr. Build. Mater.* **2023**, *368*, 130389. [[CrossRef](#)]
15. Behera, M.; Bhattacharyya, S.-K.; Minocha, A.-K.; Deoliya, R.; Maiti, S. Recycled aggregate from C&D waste & its use in concrete—A breakthrough towards sustainability in construction sector: A review. *Constr. Build. Mater.* **2014**, *68*, 501–516.
16. Yu, A.-T.W.; Poon, C.-S.; Wong, A.; Yip, R.; Jaillon, L. Impact of Construction Waste Disposal Charging Scheme on work practices at construction sites in Hong Kong. *Waste Manag.* **2013**, *33*, 138–146. [[CrossRef](#)]
17. Markssuel, M.; Paulode, M.; Erich, R.; Sergio, N.-M.; Afonso, R.-G. Recycled Aggregate: A Viable Solution for Sustainable Concrete Production. *Materials* **2022**, *15*, 5276. [[CrossRef](#)] [[PubMed](#)]
18. Li, J.-L.; Feng, Y.; Zhong, H.-C.; Zhang, B.-F.; Wang, J.-J.; Zhang, B.; Xie, J.-H. Effect of the Pretreatment on the Properties of Cement-Based Recycled Powder. *Coatings* **2024**, *14*, 107. [[CrossRef](#)]
19. Silva, R.-V.; de Brito, J.; Dhir, R.-K. Establishing a relationship between modulus of elasticity and compressive strength of recycled aggregate concrete. *J. Clean. Prod.* **2016**, *112*, 2171–2186. [[CrossRef](#)]
20. Guo, H.; Shi, C.-J.; Guan, X.-M.; Zhu, J.-P.; Ding, Y.-H.; Ling, T.-C.; Zhang, H.-B.; Wang, Y.-L. Durability of recycled aggregate concrete—A review. *Cem. Concr. Compos.* **2018**, *89*, 251–259. [[CrossRef](#)]
21. Etxeberria, M.; Vázquez, E.; Mari, A.; Barra, M. Influence of amount of recycled coarse aggregates and production process on properties of recycled aggregate concrete. *Cem. Concr. Res.* **2007**, *37*, 735–742. [[CrossRef](#)]
22. Xie, J.-H.; Li, J.-L.; Zhang, B.-F.; Chen, W.; Zhong, H.-C.; Yang, J.; Yu, T.; Feng, Y. Effects of pretreated recycled fine aggregates on the mechanical properties and microstructure of alkali-activated mortar. *Case Stud. Constr. Mater.* **2024**, *20*, e02819. [[CrossRef](#)]
23. Zhang, H.-R.; Ji, T.; Zeng, X.P.; Yang, Z.-X.; Lin, X.-J.; Liang, Y.-N. Mechanical behavior of ultra-high performance concrete (UHPC) using recycled fine aggregate cured under different conditions and the mechanism based on integrated microstructural parameters. *Constr. Build. Mater.* **2018**, *192*, 489–507. [[CrossRef](#)]
24. Xiao, J.-Z.; Li, W.-G.; Sun, Z.-H.; Lange, D.-A.; Shah, S.-P. Properties of interfacial transition zones in recycled aggregate concrete tested by nanoindentation. *Cem. Concr. Compos.* **2013**, *37*, 276–292. [[CrossRef](#)]
25. Feng, Y.; Zhang, B.-F.; Xie, J.-H.; Xue, Z.-X.; Huang, K.-H.; Tan, J.-K. Effects of recycled sand and nanomaterials on ultra-high performance concrete: Workability, compressive strength and microstructure. *Constr. Build. Mater.* **2023**, *378*, 131180. [[CrossRef](#)]
26. Shi, X.-S.; Wang, Q.-Y.; Zhao, X.-L.; Frank, C. Discussion on Properties and Microstructure of Geopolymer Concrete Containing Fly Ash and Recycled Aggregate. *Adv. Mater. Res.* **2012**, *450–451*, 1577–1583. [[CrossRef](#)]
27. Xie, J.-H.; Wang, J.-J.; Rao, R.; Wang, C.-H.; Fang, C. Effects of combined usage of GGBS and fly ash on workability and mechanical properties of alkali activated geopolymer concrete with recycled aggregate. *Compos. Part B* **2019**, *164*, 179–190. [[CrossRef](#)]
28. Adessina, A.; Ben Fraj, A.; Barthélémy, J.-F.; Chateau, C.; Garnier, D. Experimental and micromechanical investigation on the mechanical and durability properties of recycled aggregates concrete. *Cem. Concr. Res.* **2019**, *126*, 105900. [[CrossRef](#)]
29. Al-Kheetan, M.-J.; Jweihan, Y.-S.; Rabi, M.; Ghaffar, S.-H. Durability Enhancement of Concrete with Recycled Concrete Aggregate: The Role of Nano-ZnO. *Buildings* **2024**, *14*, 353. [[CrossRef](#)]
30. Padmini, A.-K.; Ramamurthy, K.; Mathews, M.-S. Influence of parent concrete on the properties of recycled aggregate concrete. *Constr. Build. Mater.* **2009**, *23*, 829–836. [[CrossRef](#)]
31. Katz, A. Properties of concrete made with recycled aggregate from partially hydrated old concrete. *Cem. Concr. Res.* **2003**, *33*, 703–711. [[CrossRef](#)]
32. De Juan, M.-S.; Gutiérrez, P.-A. Study on the influence of attached mortar content on the properties of recycled concrete aggregate. *Constr. Build. Mater.* **2009**, *23*, 872–877. [[CrossRef](#)]
33. Nuaklong, P.; Sata, V.; Chindaprasirt, P. Influence of recycled aggregate on fly ash geopolymer concrete properties. *J. Clean. Prod.* **2016**, *112*, 2300–2307. [[CrossRef](#)]

34. Xie, J.-H.; Zhao, J.-B.; Wang, J.-J.; Fang, C.; Yuan, B.; Wu, Y.-H. Impact behaviour of fly ash and slag-based geopolymeric concrete: The effects of recycled aggregate content, water-binder ratio and curing age. *Constr. Build. Mater.* **2022**, *331*, 127359. [[CrossRef](#)]
35. Zhu, P.-H.; Hua, M.-Q.; Liu, H.; Wang, X.-J.; Chen, C.-H. Interfacial evaluation of geopolymer mortar prepared with recycled geopolymer fine aggregates. *Constr. Build. Mater.* **2020**, *259*, 119849. [[CrossRef](#)]
36. ASTM C618-22; Standard Specification for Coal Fly Ash and Raw or Calcined Natural Pozzolan for Use in Concrete. American Society Testing and Materials: West Conshohocken, PA, USA, 2023.
37. Xie, J.-H.; Chen, W.; Wang, J.-J.; Fang, C.; Zhang, B.-X.; Liu, F. Coupling effects of recycled aggregate and GGBS/metakaolin on physicochemical properties of geopolymer concrete. *Constr. Build. Mater.* **2019**, *226*, 345–359. [[CrossRef](#)]
38. Venu, M.; Rao, T.-D.G. Tie-confinement aspects of fly ash-GGBS based geopolymer concrete short columns. *Constr. Build. Mater.* **2017**, *151*, 28–35. [[CrossRef](#)]
39. Alrefaei, Y.; Wang, Y.-S.; Dai, J.-G. The effectiveness of different superplasticizers in ambient cured one-part alkali activated pastes. *Cem. Concr. Compos.* **2019**, *97*, 166–174. [[CrossRef](#)]
40. Jang, J.-G.; Lee, N.-K.; Lee, H.-K. Fresh and hardened properties of alkali-activated fly ash/slag pastes with superplasticizers. *Constr. Build. Mater.* **2014**, *50*, 169–176. [[CrossRef](#)]
41. Zhang, L.-L.; Ji, Y.-S.; Li, J.; Gao, F.-R.; Huang, G.-D. Effect of retarders on the early hydration and mechanical properties of reactivated cementitious material. *Constr. Build. Mater.* **2019**, *212*, 192–201. [[CrossRef](#)]
42. Oderji, S.-Y.; Chen, B.; Shakya, C.; Ahmad, M.-R.; Shah, S.-F.A. Influence of superplasticizers and retarders on the workability and strength of one-part alkali-activated fly ash/slag binders cured at room temperature. *Constr. Build. Mater.* **2019**, *229*, 116891. [[CrossRef](#)]
43. Revathi, T.; Jeyalakshmi, R. Fly ash–GGBS geopolymer in boron environment: A study on rheology and microstructure by ATR FT-IR and MAS NMR. *Constr. Build. Mater.* **2021**, *267*, 120965. [[CrossRef](#)]
44. Fang, G.-H.; Chen, J.-T.; Dong, B.-Q.; Liu, B. Microstructure and micromechanical properties of interfacial transition zone in green recycled aggregate concrete. *J. Build. Eng.* **2023**, *66*, 105860. [[CrossRef](#)]
45. Lloyd, R.-R.; Provis, J.-L.; van Deventer, J.-S.J. Microscopy and microanalysis of inorganic polymer cements. 1: Remnant fly ash particles. *J. Mater. Sci.* **2009**, *44*, 608–619. [[CrossRef](#)]
46. Kumar, S.; Kumar, R.; Mehrotra, S.-P. Influence of granulated blast furnace slag on the reaction, structure and properties of fly ash based geopolymer. *J. Mater. Sci.* **2010**, *45*, 607–615. [[CrossRef](#)]
47. Kumar, G.; Mishra, S.-S. Effect of GGBFS on Workability and Strength of Alkali-activated Geopolymer Concrete. *Civ. Eng. J.* **2021**, *7*, 1036–1049. [[CrossRef](#)]
48. Bakharev, T.; Sanjayan, J.-G.; Cheng, Y.-B. Resistance of alkali-activated slag concrete to acid attack. *Cem. Concr. Res.* **2023**, *33*, 1607–1611. [[CrossRef](#)]
49. Hardjito, D.; Wallah, S.-E.; Sumajouw, D.-M.J.; Rangan, B.-V. On the development of fly ash-based geopolymer concrete. *ACI Mater. J.* **2004**, *101*, 467–472.
50. Ryu, G.-S.; Lee, Y.-B.; Koh, K.-T.; Chung, Y.-S. The mechanical properties of fly ash-based geopolymer concrete with alkaline activators. *Constr. Build. Mater.* **2013**, *47*, 409–418. [[CrossRef](#)]
51. GB/T 50080-2016; Standard for Test Method Performance of Ordinary Concrete. National Technical Committee on Cement Standardization Press: Beijing, China, 2016.
52. JGJ/T70-2009; Standard for Test Method of Performance on Building Mortar. National Technical Committee on Cement Standardization Press: Beijing, China, 2009.
53. ASTM C469-02; Standard Test Method for Static Modulus of Elasticity and Poisson's Ratio of Concrete in Compression. American Society Testing and Materials: West Conshohocken, PA, USA, 2017.
54. Xie, J.-H.; Wang, J.-J.; Zhang, B.-X.; Fang, C.; Li, L.-J. Physicochemical properties of alkali activated GGBS and fly ash geopolymeric recycled concrete. *Constr. Build. Mater.* **2019**, *204*, 384–398. [[CrossRef](#)]
55. Zheng, Y.-Q.; Zheng, L.-Y.; Wang, Y.-Q. Compressive performance and stress–strain relationship of geopolymer recycled brick aggregate concrete. *Mag. Concr. Res.* **2023**, *75*, 973–983. [[CrossRef](#)]
56. Fallah, M.-A.; Mousavinejad, S.-H.G. A Comparative Study of Properties of Ambient-Cured Recycled GGBFS Geopolymer Concrete and Recycled Portland Cement Concrete. *J. Mater. Civ. Eng.* **2023**, *35*, 5022002. [[CrossRef](#)]
57. Huang, J.-G.; Zou, C.-Y.; Sun, D.; Yang, B.; Yan, J.-C. Effect of recycled fine aggregates on alkali-activated slag concrete properties. *Structures* **2021**, *30*, 89–99. [[CrossRef](#)]
58. Pasupathy, K.; Ramakrishnan, S.; Sanjayan, J. Influence of recycled concrete aggregate on the foam stability of aerated geopolymer concrete. *Constr. Build. Mater.* **2021**, *271*, 121850. [[CrossRef](#)]
59. Lee, W.-K.W.; van Deventer, J.-S.J. The effect of ionic contaminants on the early-age properties of alkali-activated fly ash-based cements. *Cem. Concr. Res.* **2002**, *32*, 577–584. [[CrossRef](#)]
60. Fan, C.-C.; Huang, R.; Hwang, H.; Chao, S.-J. Properties of concrete incorporating fine recycled aggregates from crushed concrete wastes. *Constr. Build. Mater.* **2016**, *112*, 708–715. [[CrossRef](#)]
61. Rifa, A.; Subhani, S.-M.; Bahurudeen, A.; Santhosh, K.-G. A systematic comparison of performance of recycled concrete fine aggregates with other alternative fine aggregates: An approach to find a sustainable alternative to river sand. *J. Build. Eng.* **2023**, *78*, 107695. [[CrossRef](#)]

62. Ju, M.; Park, K.; Park, W.-J. Mechanical Behavior of Recycled Fine Aggregate Concrete with High Slump Property in Normal- and High-Strength. *Int. J. Concr. Struct. Mater.* **2019**, *13*, 61. [[CrossRef](#)]
63. Sinha, A.-K.; Talukdar, S. Enhancement of the properties of silicate activated ultrafine-slag based geopolymer mortar using retarder. *Constr. Build. Mater.* **2021**, *313*, 125380. [[CrossRef](#)]
64. Venu, M.; Gunneswara Rao, T.-D. An Experimental Investigation of the Stress-Strain Behaviour of Geopolymer Concrete. *Slovak J. Civ. Eng.* **2018**, *26*, 30–34. [[CrossRef](#)]
65. Li, B.; Gao, A.-X.; Li, Y.; Xiao, H.-L.; Chen, N.; Xia, D.-T.; Wang, S.-B.; Li, C.-N. Effect of silica fume content on the mechanical strengths, compressive stress–strain behavior and microstructures of geopolymeric recycled aggregate concrete. *Constr. Build. Mater.* **2023**, *384*, 131417. [[CrossRef](#)]
66. Xie, J.-H.; Huang, L.; Guo, Y.-C.; Li, Z.-J.; Fang, C.; Li, L.-J.; Wang, J.-J. Experimental study on the compressive and flexural behaviour of recycled aggregate concrete modified with silica fume and fibres. *Constr. Build. Mater.* **2018**, *178*, 612–623. [[CrossRef](#)]
67. Gesoglu, M.; Güneysi, E.; Öz, H.-Ö.; Taha, I.; Yasemin, M.-T. Failure characteristics of self-compacting concretes made with recycled aggregates. *Constr. Build. Mater.* **2015**, *98*, 334–344. [[CrossRef](#)]
68. Geng, J.; Chen, Y.-Y.; Sun, J.-Y.; Chen, W. Basic Mechanics Characters of Recycled Fine Aggregate Concrete. *Adv. Mater. Res.* **2012**, *446–449*, 2028–2032. [[CrossRef](#)]
69. Hasnaoui, A.; Ghorbel, E.; Wardeh, G. Performance of metakaolin/slag-based geopolymer concrete made with recycled fine and coarse aggregates. *J. Build. Eng.* **2021**, *42*, 102813. [[CrossRef](#)]
70. Shi, C.-J.; Li, Y.-K.; Zhang, J.-K.; Li, W.-G.; Chong, L.-L.; Xie, Z.-B. Performance enhancement of recycled concrete aggregate—A review. *J. Clean. Prod.* **2016**, *112*, 466–472. [[CrossRef](#)]
71. Dilbas, H.; Simsek, M.; Çakir, Ö. An investigation on mechanical and physical properties of recycled aggregate concrete (RAC) with and without silica fume. *Constr. Build. Mater.* **2014**, *61*, 50–59. [[CrossRef](#)]
72. Zhang, M.-M.; Zhu, L.-H.; Gao, S.; Dong, Y.-R.; Yuan, H.-Q. Mechanical properties of recycled aggregate concrete prepared from waste concrete treated at high temperature. *J. Build. Eng.* **2023**, *76*, 107045. [[CrossRef](#)]
73. Li, J.; Chen, L.-L.; Wang, Z.-F.; Wang, Y.-Q. Effect of Modification and Replacement Rate of Recycled Coarse Aggregate on Properties of Recycled Aggregate Concrete. *Iran. J. Sci. Technol.* **2023**, *47*, 3321–3332. [[CrossRef](#)]
74. Fang, C.-L.; Feng, J.-C.; Huang, S.-S.; Hu, J.; Wang, W.; Li, N. Mechanical properties and microscopic characterization of mortar with recycled aggregate from waste road. *Case Stud. Constr. Mater.* **2022**, *17*, e01441. [[CrossRef](#)]
75. Hu, Y.; Tang, Z.; Li, W.-G.; Li, Y.-N.; Tam, V.-W.Y. Physical-mechanical properties of fly ash/GGBFS geopolymer composites with recycled aggregates. *Constr. Build. Mater.* **2019**, *226*, 139–151. [[CrossRef](#)]
76. *ACI 318-19; Building Code Requirements for Structural Concrete and Commentary*. American Concrete Institute: Indianapolis, IN, USA, 2019.
77. Collins, M.-P.; Mitchell, D.; Macgregor, J.-G. Structural Design Considerations for High-Strength Concrete. *Concr. Int.* **1993**, *15*, 27–34.
78. Noushini, A.; Aslani, F.; Castel, A.; Gilbert, R.-I.; Uy, B.; Foster, S. Compressive stress-strain model for low-calcium fly ash-based geopolymer and heat-cured Portland cement concrete. *Cem. Concr. Compos.* **2016**, *73*, 136–146. [[CrossRef](#)]
79. *CEB-FIP Model Code 2010: Design Code*; Comité Euro-International Du Béton: Lausanne, Switzerland, 2013.
80. Xiao, J.-Z.; Li, J.-B.; Zhang, C. Mechanical properties of recycled aggregate concrete under uniaxial loading. *Cem. Concr. Res.* **2005**, *35*, 1187–1194. [[CrossRef](#)]
81. Chang, Y.-C.; Wang, Y.-Y.; Zhang, H.; Chen, J.; Geng, Y. Different influence of replacement ratio of recycled aggregate on uniaxial stress-strain relationship for recycled concrete with different concrete strengths. *Structures* **2022**, *42*, 284–308. [[CrossRef](#)]
82. Li, B.; Wu, F.; Xia, D.-T.; Li, Y.; Cui, K.; Wu, F.-H.; Yu, J.-L. Compressive and flexural behavior of alkali-activated slag-based concrete: Effect of recycled aggregate content. *J. Build. Eng.* **2023**, *67*, 105993. [[CrossRef](#)]

Disclaimer/Publisher’s Note: The statements, opinions and data contained in all publications are solely those of the individual author(s) and contributor(s) and not of MDPI and/or the editor(s). MDPI and/or the editor(s) disclaim responsibility for any injury to people or property resulting from any ideas, methods, instructions or products referred to in the content.